High-angular-momentum states in ^{106}Ag and their rotational interpretation

Rakesh Popli, F. A. Rickey, L. E. Samuelson,* and P. C. Simms
Tandem Accelerator Laboratory, Purdue University, West Lafayette, Indiana 47907
(Received 8 August 1980)

Levels in ^{106}Ag have been studied using heavy-ion reactions. The experiments included γ-ray yields as a function of bombarding energy, γ-ray angular distributions, γ-ray linear polarizations, and three-detector γ-γ coincidence measurements. The decay scheme includes four collective bands with low-lying bandheads. The energies, γ-ray mixing ratios, and branching ratios of states in these bands are shown to be in good agreement with the corresponding quantities calculated using a two-particles-plus-rotor model at a small, symmetric deformation ($\delta = 0.12$). The Coriolis and recoil effects are explicitly included and a variable moment of inertia is used. The calculation also shows that the four bands have predominant configurations $\nu(d_{5/2}) \otimes \pi(g_{9/2})$, $\nu(g_{7/2}) \otimes \pi(g_{9/2})$, $\nu(h_{11/2}) \otimes \pi(p_{1/2})$, and $\nu(h_{11/2}) \otimes \pi(g_{9/2})$, respectively. The $\Delta I = 1$ and $\Delta I = 2$ level sequences in the bands can be understood on the basis of the positions of the neutron and proton Fermi surfaces in the respective Nilsson bases. Another band observed experimentally on a 10^- bandhead at 2.4416 MeV is thought to have a four-quasiparticle structure.

[NUCLEAR STRUCTURE ^{96}Zr(^{14}N, $4n$)^{106}Ag at 49 MeV: measured $I_\gamma[E(^{14}\mathrm{N})]$, $I_\gamma(\theta)$, P_γ, γ-γ coin., γ-γ DCOQ. ^{106}Ag deduced levels, J, π, γ mixing ratios. Two-particle-plus-rotor calculations, Coriolis. Calculated levels, mixing ratios, branching ratios, lifetimes. Ge(Li) detectors.]

I. INTRODUCTION

The widespread observation of band structure in transitional nuclei suggests that collective models might be appropriate even for nuclei near closed shells. The symmetric-rotor model is an attractive choice because its features and systematics have been established by investigations of strongly deformed nuclei. This model has been used successfully to describe collective bands in odd-A (Refs. 1–4) and even-even[5] nuclei in the mass-100 region. The purpose of the present work is to study the structure of the odd-odd nucleus ^{106}Ag and to see if it can be interpreted in the same framework. Odd-odd nuclei are challenging because they combine the features of odd-neutron and odd-proton nuclei into a more complex system.

Some features of transitional nuclei might seem inconsistent with a symmetric-rotational description. For example, deviations from the $I(I+1)$ energy pattern occur at lower spins in transitional nuclei than in strongly deformed nuclei. However, this difference is consistent with recent experiments[6] which indicate that the deviations in strongly deformed nuclei are due to Coriolis antipairing, and this effect would be more significant in slightly deformed nuclei. A second question concerns excited states of the core (0_2^+, 2_2^+, etc.) which are missing in the rotational description. Similar states, i.e., the beta and gamma vibrations, occur in strongly deformed nuclei but are assumed to be independent because of the large differences between vibrational and rotational energies. This independence is not expected for transitional nuclei where the rotational energies are much larger. Nevertheless, our calculation, which ignores nonrotational states of the core, is in excellent agreement with a wide variety of data for states near the yrast line.

Until very recently, nothing was known of the high-spin states in ^{106}Ag except for an isomeric state of spin-parity 6^+. Samuelson *et al.*,[7] using the ^{103}Rh$(\alpha, n\gamma)^{106}$Ag and ^{104}Pd$(\alpha, pn\gamma)^{106}$Ag reactions, have presented a level scheme of ^{106}Ag up to 2253.73 keV in energy and 12 in spin. In the present paper, a detailed analysis of the ^{96}Zr(^{14}N, $4n\gamma$) reaction leading to the ^{106}Ag nucleus is presented and the limited level scheme of Samuelson *et al.* is extended considerably. Four collective bands have been observed which are in agreement with a two-quasiparticle-plus-rotor calculation of energies, wave functions, and transition properties. A fifth band beginning at approximately 2.5 MeV has also been observed and is thought to have a four-quasiparticle structure.

II. EXPERIMENTAL PROCEDURES

Most of the data were obtained with the reaction ^{96}Zr(^{14}N, $4n$)^{106}Ag at a beam energy of 49 MeV. The ^{14}N beam was obtained from the Purdue Tandem Van de Graaff accelerator. The isotope ^{107}Ag was also produced in the same experiment by the evaporation of three neutrons. The experimental procedures used for taking and an-

alyzing data have been described in our recent publication[4] on ^{105,107}Ag and in previous papers[8,9]; therefore, only a brief summary will be given here. The measurements included γ-ray intensities as a function of beam energy, γ-ray angular distributions,[8] three detector γ-γ coincidences,[9] and γ-ray linear polarizations. In addition, coincidence data from ^{97}Mo(^{12}C,$p2n$)^{106}Ag at 45 MeV and several other heavy-ion reactions were used to confirm the assignment of γ rays to ^{106}Ag and to remove ambiguities in the decay scheme.

Enriched targets and Ge(Li) detectors with energy resolutions from 2.1 to 2.5 keV [full width at half maximum (FWHM) at a γ-ray energy of 1333 keV] were used. The ^{14}N reaction yielded many product nuclides,[4] but more ^{106}Ag was produced than any other nuclide. The coincidence data were recorded event by event on magnetic tape and later sorted and analyzed using a PDP-15 computer. The positions of the three detectors were such that the data could be used to extract γ-ray singles intensities and also to determine multipolarities and mixing ratios by the directional correlation from oriented nuclei referred to quadrupole transitions (DCOQ) method.[10] A specimen singles spectrum is shown in Fig. 1.

The γ-ray linear polarizations were obtained by measuring γ-ray Compton scattering in directions parallel and perpendicular to the beam direction.[11] A special polarimeter was not necessary. Instead, two conventional Ge(Li) detectors were placed together on a turntable with the midpoint of the straight line joining the crystals vertically below the target at a distance of 13.5 cm. Pulses from the two detectors were

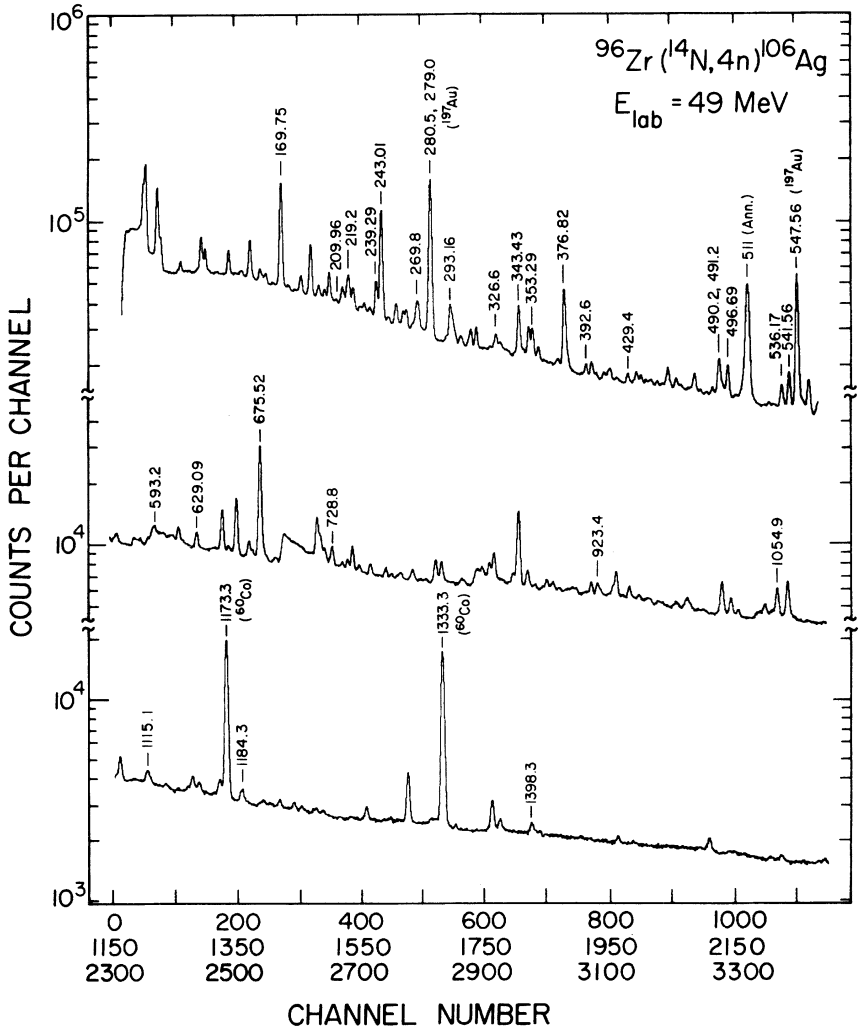

FIG. 1. Singles spectrum from the ^{96}Zr(^{14}N,$4n$)^{106}Ag reaction. This represents a weighted sum of all singles spectra taken at different detector angles.

fed into separate analog-to-digital converters (ADC's) (with a 30 nsec coincidence requirement). Energy summation was performed in the computer after nonlinearity corrections to avoid loss of energy resolution caused by nonlinearities in the two detector channels. In this arrangement, the gains and biases of the two amplifiers did not have to be matched precisely. A resolution of 3.1 keV (FHWM at 1333 keV) was obtained.

The γ-ray polarization was calculated from

$$P_{\text{exp}} = \frac{1}{Q} \cdot \frac{N(90°) - N(0°)}{N(90°) + N(0°)},$$

where $N(90°)$ and $N(0°)$ denote γ-ray count rates with the scattering axis perpendicular and parallel, respectively, to the beam direction. Q is the efficiency of the polarimeter as determined from data taken for γ rays of known polarization. Figure 2 shows the efficiency calibration of the polarimeter. The large error bars reflect the fact that the calibration was run for a relatively short time—125 min in each of the two orientations. The efficiency obtained here with a pair of conventional detectors is similar to that obtained by Kim *et al.*[11] using a special polarimeter.

III. LEVEL SCHEME

A. General

Gamma-ray cascades were assigned to ^{106}Ag on the basis of the γ-ray intensities measured following various heavy-ion reactions.[4] The ^{96}Zr + ^{14}N reaction could have yielded only Rh, Pd, or Ag isotopes. The 170-676-377-keV, 243-293-keV, and 239-393-keV cascades produced in this reaction were also observed following the ^{97}Mo + ^{12}C and ^{92}Zr + ^{16}O reactions which could not have produced Rh isotopes. Ruling out Pd on the basis of known decay schemes for all relevant Pd isotopes, we concluded that these cascades must belong to Ag isotopes. As described in detail in Ref. 4, the relative intensities of these and other cascades (assigned to ^{107}Ag) following the ^{94}Zr + ^{16}O and ^{97}Mo + ^{12}C reactions proved that the former belonged to ^{106}Ag. These assignments are confirmed by the recent (α, n) and (α, pn) work of Samuelson *et al.*[7]

The proposed level scheme for ^{106}Ag is shown in Figs. 3 and 4. Sixty-four γ rays connecting 40 high-angular-momentum states have been included. A number of low-angular-momentum states decaying eventually into the 1^+ ground state were also observed. These were found to be consistent with the level scheme given by Samuelson *et al.*, and therefore are not shown here.

Table I presents the results of the angular distribution, DCOQ, and linear polarization analyses for the γ rays connecting the high-angular-momentum states. It is apparent from Table I that there is a substantial interference between many γ rays in the singles spectrum (γ rays with superscripts b and c in column 1). Therefore, the γ-γ coincidence data were used to determine precise energies, intensities, multipolarities, and mixing ratios for many γ rays.

The parameters A_{kk} listed in columns 4 and 5 of Table I were obtained by fitting the angular

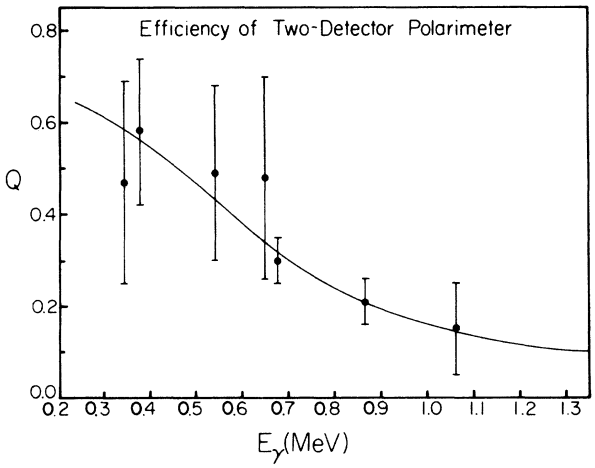

FIG. 2. Efficiency of the simple two-detector polarimeter as a function of γ-ray energy.

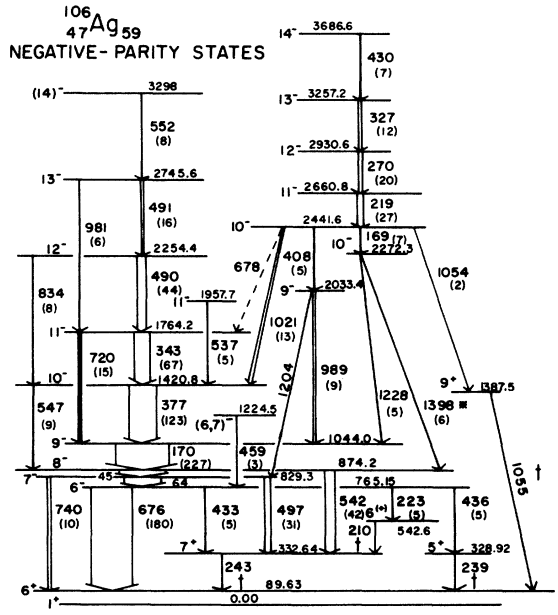

FIG. 3. Decay scheme for the negative-parity states in ^{106}Ag. Low-spin states are not shown. Transitions between positive-parity states, marked with a † sign, are also shown in Fig. 4.

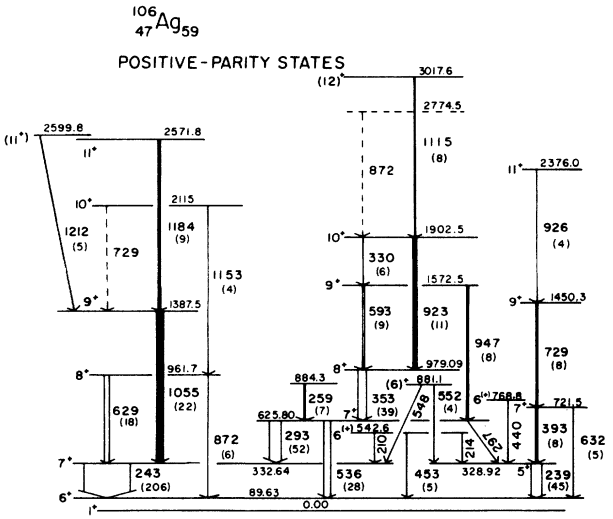

FIG. 4. Decay scheme for the positive-parity states in ^{106}Ag. Low-spin states are not shown.

distribution data to the usual function

$$W(\theta) = A_0 Q_0 \left[1 + A_{22}\frac{Q_2}{Q_0} P_2(\cos\theta) + A_{44}\frac{Q_4}{Q_0} P_4(\cos\theta)\right],$$

where the Q_k are solid angle correction factors. The effect of nuclear deorientation, due to emission of particles and γ rays, is included in the distribution coefficients by the parameters α_k defined by

$$A_{kk} = \alpha_k A^0_{kk},$$

where A^0_{kk} can be calculated for known spin changes and mixing ratios from the data tabulated by Yamazaki.[12] The usual method[8] of determining α_k's is to first identify some intense, pure $E2$ transitions and calculate α_k for those from the A_{kk} and A^0_{kk} values. Then the α_k's for other transitions can be obtained by relating them to the corresponding coefficients for the neighboring $E2$ transitions. In the present case, however, there were no strong $E2$ transitions. Therefore, the values of parameters α_k at the top of each band were estimated from systematics in this region of nuclei ($\alpha_2 \approx 0.8$). Then α_k's for other states were calculated using the deorientation caused by observed γ rays.

The DCOQ analysis[10] was very useful in determining the multipolarities and mixing ratios of γ rays not resolved in the singles. The number R_{DCOQ} listed in Table I is basically a measure of the anisotropy of the γ ray relative to that of a pure quadrupole transition. R_{DCOQ} (γ_1) for transition γ_1 is evaluated from the γ_1-γ_2 coincidence data where γ_2 is either a quadrupole transition or any other kind with a known anisotropy relative to a quadrupole transition. Since there were no strong $E2$ transitions in this nucleus, the following procedure was adopted. A few "standard" transitions near the bottom of each band were selected, which were intense and clearly resolved in the singles. The R_{DCOQ} value for each of these was calculated *theoretically*, based on its spin sequence and mixing ratio obtained from angular distribution analysis. Then the R_{DCOQ} for other γ rays (γ_1) in coincidence with any of these standard γ rays (γ_2) could be determined by the usual procedure.

Columns 10 and 11 of Table I list P_{exp} and P_{ad}, the measured and predicted values, respectively, of the γ-ray polarization. P_{ad} is calculated from the angular distribution coefficients as

$$P_{ad} = \frac{3A_{22}H_2(\delta) + 1.75A_{44}}{2 - A_{22} + 0.75A_{44}},$$

where H_2 is a function of the spin sequence and mixing ratio.[11] The sign of the ratio P_{exp}/P_{ad} determines the parity relationship: a negative sign implies a change in parity, whereas a positive sign implies no parity change. The magnitude of P_{exp}/P_{ad} should be equal to 1 within the limits of error. If the magnitude and sign of this ratio and the mixing ratio δ are not consistent, it indicates that the mixing ratio and/or the spin sequence is wrong. Thus, the polarization data can also be useful in removing ambiguities in spin assignments and mixing ratios, besides determining parities.

B. Placement of γ rays

The coincidence data implied that the 676-keV γ ray must be placed at the bottom of the 377-170-676-keV cascade (Fig. 3) and there must be no other coincidence γ ray beneath it. This suggested that this γ ray populated the 1^+ ground state or the 6^+ metastable state at 89.63 keV, both known from previous work.[13,7] Since heavy-ion reactions such as the ones described above are not expected to populate low-angular-momentum states strongly, we have considered the 676-keV γ ray as populating the 6^+ state. This is consistent with the observation[14] of a state at 769 keV in the reaction ^{104}Pd$(\alpha, d)^{106}$Ag with an angular momentum transfer of 5.

The rest of the γ rays shown in Fig. 3 were placed on the basis of coincidence relationships. Some weak γ rays were also helpful in removing ambiguities. For example, the 243-keV line was strongly in coincidence with 170- and 377-keV lines and other lines above the 874.2-keV state, but not with the 676-keV line. The possibility of a 243-keV line depopulating the 874.2-keV state (in which case the order in the 45-64-676-

TABLE I. Analysis for γ rays emitted following the $^{96}Zr(^{14}N,4n)^{106}Ag$ reaction at 49 MeV. Where more than one possible spin relationship is shown for any transition, the first one is the adopted one.

Energy (keV)	$I_i^\pi \rightarrow I_f^\pi$	Relative intensity	A_{22}	A_{44}	α_2	α_4	R_{DCOQ}	δ	P_{exp}	P_{ad}	Parity change
169.75(5)	$9^- \rightarrow 8^-$	227(1) [a]	−0.162(13)	−0.021(15)	0.77(6)	0.44(9)		0.04(2) [d]			
170.0(2)	$10^- \rightarrow 10^-$	7(1) [c]									
209.96(8)	$6^{(+)} \rightarrow 7^+$	3.1(2) [a]	−0.320(172)	0.151(226)	0.69(7)	0.34(8)		0.2(2) [d]			
213.68(8)	$6^{(+)} \rightarrow 5^+$	5.9(5) [c]					2.3(5)	−0.03(9) [e]			
219.2(1)	$11^- \rightarrow 10^-$	20(1) [b]	−0.128(22)	0.041(29)	0.80(8)	0.51(15)	1.8(1)	0.06(2) [d,e]			
222.5(1)	$6^- \rightarrow 6^{(+)}$	5(1) [c]									
239.29(5)	$5^+ \rightarrow 6^+$	45.5(5) [a]	−0.156(11)	−0.017(14)	0.69(8)	0.32(10)		0.02(2) [d]			
243.01(6)	$7^+ \rightarrow 6^+$	206(8) [b]	−0.415(12)	−0.021(9)	0.72(7)	0.36(10)	3.2(1)	−0.15(2) [d,e]			
258.5(2)	$\rightarrow 7^+$	7.2(6) [c]									
269.8(1)	$12^- \rightarrow 11^-$	19.7(5) [b]	−0.058(30)	−0.060(37)	0.81(8)	0.53(15)	1.5(1)	0.11(2) [d,e]			
293.16(8)	$7^+ \rightarrow 7^+$	52(2) [b]	0.277(12)	0.031(17)	0.70(6)	0.33(8)		−0.17(8) [d]	0.56(20)	0.85(10) [g]	No
	$8^+ \rightarrow 7^+$							0.37(4)		−0.57(7) [g]	Yes
296.9(2)	$7^+ \rightarrow 5^+$	3.1(5) [c]									
326.6(1)	$13^- \rightarrow 12^-$	11.9(3) [b]	−0.013(34)	0.013(45)	0.81(8)	0.53(15)	1.7(2)	0.08(5) [e]			
330.0(2)	$10^+ \rightarrow 9^+$	6(1) [c]									
343.43(6)	$11^- \rightarrow 10^-$	67.1(5) [a]	−0.236(11)	0.024(12)	0.79(7)	0.49(13)	2.14(9)	0.00(2) [d,e]	−0.24(10)	−0.30(6)	No
353.29(7)	$8^+ \rightarrow 7^+$	38.7(4) [a]	−0.129(19)	−0.014(23)	0.72(7)	0.37(10)		0.05(2) [d]	−0.15(14)	−0.32(9)	No
376.82(9)	$10^- \rightarrow 9^-$	122.8(5) [a]	−0.168(8)	0.006(8)	0.78(7)	0.46(12)		0.04(2) [d]	−0.36(5)	−0.36(9)	No
392.6(3)	$7^+ \rightarrow 5^+$	7.5(6) [b]	0.201(40)	−0.079(54)	0.75(8)	0.41(12)					
408.2(2)	$10^- \rightarrow 9^-$	7.5(6) [b]	−0.119(65)	0.122(92)	0.80(7)	0.50(13)		0.07(5) [d]			
429.4(2)	$14^- \rightarrow 13^-$	6.8(4) [b]	−0.020(57)	−0.020(69)	0.82(8)	0.55(15)	2.1(4)	0.08(6) [d,e]			
432.5(1)	$6^- \rightarrow 7^+$	5(1) [c]					1.9(3)	0.01(8) [e]			
436.2(1)	$6^- \rightarrow 5^+$	5(1) [a]	−0.410(112)	0.348(164)	0.70(6)	0.33(8)					
439.9(2)	$6^{(+)} \rightarrow 5^+$	5.6(2) [a]	−0.369(119)	0.302(163)	0.70(6)	0.33(8)		0.15(5) [d]			
453.0(1)	$6^{(+)} \rightarrow 6^+$	5.5(8) [c]									
459.4(3)	$\rightarrow 6^-$	3(1) [c]									
490.2(2)	$12^- \rightarrow 11^-$	44(1) [b]	−0.249	0.016(49)	0.80(7)	0.50(13)			−0.51(11)	−0.27(12)	No
491.2(5)	$13^- \rightarrow 12^-$	15.9(8) [b]	0.083(124)	−0.112(125)	0.81(8)	0.52(15)					
496.69(7)	$7^- \rightarrow 7^+$	30.6(6) [a]	0.454(27)	0.010(35)	0.73(6)	0.37(8)	0.77(8)	0.8(2) [d–f]	−0.26(12)	0.26(12) [g]	Yes
	$8 \rightarrow 7^+$							0.6(1) [d,e]		−0.72(20) [g]	
536.17(9)	$7^+ \rightarrow 6^+$	28(2) [b]	0.372(39)	0.203(53)	0.70(6)	0.33(8)	7(2)	≈0.5 [d]	−0.33(16)	−0.19(7)	No
536.9(2)	$11^- \rightarrow 10^-$	5.3(7) [c]					5(2)	−0.3(2) [e]			
541.56(6)	$8^- \rightarrow 7^+$	42(1) [a]	−0.217(17)	−0.008(21)	0.75(5)	0.41(8)		0.00(2) [d]	0.34(12)	−0.30(6)	Yes
546.6(2)	$10^- \rightarrow 8^-$	9(2) [c]									
548.4(2)	$(6)^+ \rightarrow 7^+$	4(1) [c]					4(1)				
552.1(2)	$(6)^+ \rightarrow 5^+$	3.8(7) [c]					4(2)				
552.2(3)	$(14)^- \rightarrow 13^-$	7.6(9) [b]	0.268(75)	0.041(103)	0.82(8)	0.55(15)		0.34(8) [d]			
593.2(2)	$9^+ \rightarrow 8^+$	9(1) [a]	−0.286(119)	0.729(216)	0.73(8)	0.38(11)		0.15(10) [d]			
629.09(9)	$8^+ \rightarrow 7^+$	18(2) [a]	0.172(36)	0.216(50)	0.70(6)	0.34(8)		6(2) [d]			

TABLE I. (*Continued.*)

Energy (keV)	$I_i^\pi \rightarrow I_f^\pi$	Relative intensity	A_{22}	A_{44}	α_2	α_4	R_{DCOQ}	δ	P_{exp}	P_{ad}	Parity change
631.9(4)	$7^+ \rightarrow 6^+$	5(2) [a]	1.099(392)	−0.212(711)	0.75(8)	0.41(12)					
675.52(5)	$6^- \rightarrow 6^+$	180(2) [b]	0.334(10)	0.036(10)	0.70(6)	0.33(8)		0.00(13) [d]	−0.58(5)	0.62(9) [g]	Yes
	$7 \rightarrow 6^+$							0.43(5)		−0.61(19) [g]	No
720.2(2)	$11^- \rightarrow 9^-$	15.0(8) [b]	0.218(26)	−0.019(43)	0.79(7)	0.49(13)			0.25(19)	0.36(7)	No
728.8(3)	$9^+ \rightarrow 7^+$	8(1) [b]	0.247(45)	0.005(65)	0.77(7)	0.45(11)					
739.7(1)	$7^- \rightarrow 6^+$	10(1) [a]	−0.468(70)	−0.212(101)	0.73(6)	0.38(9)	2.2(6)	−0.06(14) [d,e]	0.57(5)	−0.49(30)	Yes
833.7(3)	$12^- \rightarrow 10^-$	8(1) [b]	0.281(46)	−0.059(63)	0.80(7)	0.50(13)					
872.00(8)	$8^+ \rightarrow 6^+$	6(2) [b]	0.267(73)	0.038(86)	0.70(6)	0.34(8)			0.65(57)	0.48(18)	No
923.4(2)	$10^+ \rightarrow 8^+$	11(1) [a]	0.179(95)	0.004(111)	0.77(7)	0.45(11)					
925.7(1)	$11^+ \rightarrow 9^+$	4.1(2) [a]	0.302(195)	−0.063(214)	0.80(7)	0.50(13)					
946.7(2)	$9^+ \rightarrow 7^+$	8(1) [a]	0.288(149)	0.132(236)	0.73(8)	0.38(11)					
981.2(7)	$13^- \rightarrow 11^-$	6.0(7) [a]	0.487(354)	−0.397(482)	0.81(8)	0.52(15)					
989.4(4)	$9^- \rightarrow 9^-$	9.4(3) [a]	0.233(83)	−0.259(107)	0.79(7)	0.48(13)	1.2(3)				
1020.8(1)	$10^- \rightarrow 10^-$	13.2(4) [a]	0.235(186)	−0.370(361)	0.80(8)	0.51(16)	1.0(2)	$-0.44 \leq \delta \leq -0.06$; $0.4 \leq \delta \leq 0.9$			
	$8^- \rightarrow 10^-$										
1054.0(5)	$10^- \rightarrow 9^+$	1.7(7) [c]									
1054.9(1)	$9^+ \rightarrow 7^+$	22(1) [b]	0.204(35)	0.033(48)	0.73(8)	0.38(11)	1.3(1)	0.00	0.46(38)	0.36(9) [g]	No
	$8 \rightarrow 7^+$							0.31(5) [d]		−0.51(28) [g]	Yes
1115.1(4)	$(12)^+ \rightarrow 10^+$	8(1) [b]	0.007(58)	0.229(84)	0.80(7)	0.50(13)					
1153(1)	$10^+ \rightarrow 8^+$	4(1) [b]	0.536(100)	−0.196(118)	0.75(8)	0.43(12)					
1184.3(4)	$11^+ \rightarrow 9^+$	8.5(3) [a]	0.211(92)	−0.035(143)	0.78(8)	0.47(14)					
1204.2(4)	$9^- \rightarrow 7^-$	2.9(3) [a]	0.107(261)	−0.286(351)							
1212.2(3)	$(11^+) \rightarrow 9^+$	4.5(3) [a]	0.593(193)	−0.241(291)	0.78(8)	0.47(14)					
1228.4(1)	$10^- \rightarrow 9^-$	4.6(2) [a]	−0.799(172)	0.057(235)				−0.5(3) [d]			
1398.3(3)	$10^- \rightarrow 8^-$	6.3(3) [a]	−0.044(96)	0.016(129)	0.78(8)	0.47(14)					

[a] Singles and coincidence intensities are mutually consistent.
[b] Interference in singles from γ ray(s) of smaller intensity. Coincidence intensity adopted.
[c] Interference in singles from γ ray(s) of comparable or greater intensity. Angular distribution is not useful in this case.
[d] Angular distribution used to determine mixing ratio.
[e] DCOQ used to determine mixing ratio.
[f] Polarization used to determine mixing ratio.
[g] Assignment discussed in the text.

keV cascade would be reversed) was ruled out by the presence of the weak 223- and 210-keV lines and their coincidence properties.

The 219-, 270-, 327-, and 430-keV γ rays were seen to be in coincidence with one another and with the 170-676-keV cascade. They were also seen in weak coincidence with the 377-keV γ ray and many high-energy γ rays. It would appear at first that the cascade of the above-mentioned four γ rays was based on the 1044.0-keV level, but such a scheme could not be reconciled *quantitatively* with all aspects of the coincidence data, even assuming the 377-keV and some other lines to be doublets. The arrangement with the bandhead placed at 2441.6 keV and decaying by five weak branches, shown in Fig. 3, was the only one consistent with the data. This illustrates the importance of carefully corrected, quantitative coincidence data.

The relative positions of γ rays in the 219-270-327-430-keV cascade were decided by γ-ray intensities. In the case of the 170-377-344-490-491-keV cascade, the order of γ rays was unambiguous because of the existence of crossover γ rays.

The data showed each of the 170- and 1055-keV lines (Fig. 3) being in coincidence with itself. Hence, it was concluded that both were doublets. The weaker parts of these doublets were placed below the 2441.6-keV level because that was consistent with energy as well as coincidence relationships. The asterisk beside the 1398-keV line in Fig. 3 indicates that its position in the decay scheme is ambiguous. The coincidence relationships and energy sums would be equally well satisfied if this line were placed between the 1044.0- and 2441.6-keV levels, but the intensity consideration favors the arrangement shown.

The 239-keV line (Fig. 4) was placed on the basis of coincidence and energy-sum relationships with the 214- and 552-keV γ rays. This assignment is consistent with the observation of a state at 329 keV in particle-transfer data.[15] The placement of the rest of the γ rays shown in Fig. 4 followed from the coincidence data in a straightforward way.

C. Spin and parity assignments

The spin-parities of the ground state (1^+) and the isomer at 89.63 keV (6^+) were known from previous work.[13] The remaining assignments were made upward from the 6^+ isomer. Table I presents the angular distribution, DCOQ, and polarization analyses, on the basis of which the spin-parity relationships were determined. These measurements determine the angular momentum change associated with a transition but cannot distinguish between an increase and a decrease. The ambiguity can usually be removed for transitions observed following heavy-ion reactions by the yrast argument, i.e., at a given energy, the state with the highest spin is preferentially populated. This argument is particularly strong where the transition energy is high or the spin change is 2 units. Thus, for example, if there is a $\Delta I=2$ transition populating a state with spin I_f, the spin of the initial state is much more likely to be I_f+2 than I_f-2.

It has been observed in ^{106}Ag and other nuclei in this region that, in general, parity-changing transitions are highly retarded and cannot compete with $M1$ or $E2$ transitions of comparable energy. This observation was used to assign parities tentatively in a few cases discussed below.

An example of the usefulness of polarization data is provided by the 497-keV γ ray (Fig. 3). Its angular distribution and R_{DCOQ} are consistent with both $\Delta I=0$ and $\Delta I=1$ mixed transitions. The sign of the measured polarization is consistent with a parity-nonchanging $\Delta I=1$, but the magnitude is not. In the $\Delta I=0$ case, the angular distribution and R_{DCOQ} are consistent with any mixing ratio between 0.0 and 0.8. The corresponding values of P_{ad} vary from 0.88 to 0.23. Hence, the polarization data $[P_{\mathrm{exp}}=-0.26(12)]$ require a parity changing, $\Delta I=0$ transition with $\delta\approx 0.8$. An $E1$-$M2$ transition with such a high mixing ratio is highly unusual and would normally cause doubts. In the present case, however, the branching at the 829.3-keV state, 15% for 497-keV and 85% for 64-keV γ rays, in spite of the energy difference, indicates that the $E1$ transition (497- keV) is strongly retarded. Hence a significant $E1$-$M2$ mixing is not surprising. Some other assignments which may not be immediately clear from Table I are discussed below.

1044.0- and 1420.8-keV states. The energy of the 170-keV γ ray (Fig. 3) was too small for polarization measurement. Therefore the parity relationships were deduced as follows. The yrast argument indicates a $\Delta I=-1$ nature for the 170- and 377-keV γ rays (angular distribution data show that $|\Delta I|=1$ for both); hence the 874.2- and 1420.8-keV states differ in spin by 2 units. The observation of the 547-keV transition between them in the coincidence data indicates that the 1420.8-keV state has the same parity as the 874.2-keV state, i.e., negative. Since polarization data show that the 377-keV transition does not change parity, the 1044.0-keV state too must have a negative parity.

1224.5-keV state. Excitation function systema-

tics of Samuelson *et al.*[7] suggest 6 and 7 as the possible spin values for this state. Since it decays to a negative-parity state (Fig. 3), it is likely to have a negative parity.

2441.6-keV state. The angular distributions of the 1021- and 408-keV transitions require the spin of this state to be 10 or 8. The latter possibility is unlikely because of the yrast argument. The decay pattern of this state strongly suggests that it has a negative parity. A negative parity is also consistent with the rather large mixing ratio of the 1021-keV transition.

542.6-keV state. The angular distribution of the 210-keV transition (Fig. 3) implies spin 6 for this state, but leaves the parity ambiguous. However, possible transitions to this state from the negative-parity states 8^- (874.2 keV) and 7^- (829.3 keV) were not observed, even though these transitions would be favored over the 45- and 64-keV transitions by the energy factor. This suggested that the parity of the state was likely to be positive.

625.80-keV state. The data for the 293-keV γ ray (Fig. 4) are consistent with both $\Delta I=0$ without parity change, and $\Delta I=1$ with parity change. However, the 536-keV transition is definitely a mixed $\Delta I=1$ because it has a large, positive A_{44}. Hence the spin-parity of the 625.80-keV state is 7^+.

1387.5-keV state. The angular distribution of the 1055-keV transition is consistent with a mixed $\Delta I=1$ transition as well as a $\Delta I=2$ transition. In the former case, the transition would be expected to be parity-nonchanging because of its substantial mixing ratio. However, the polarization data are inconsistent with a parity-nonchanging $\Delta I=1$ transition. Thus, a spin-parity of 9^+ is assigned to the 1387.5-keV state.

3017.6-keV state. The angular distribution of the 1115-keV γ ray has probably been distorted by Doppler shift. However, the energy-spacing pattern in the band based on the 7^+ state at 625.80 keV suggests that this state may have spin 12.

D. Salient features

Various band structures are quite evident in Figs. 3 and 4, implying a collective behavior. As will be shown in Sec. V, the energies and transition properties of these bands are reproduced by a rotational model, except the band based on the 10^- state at 2441.6 keV (Fig. 3). In Fig. 4, three bands of positive-parity states can be seen. The $\Delta I=2$ band based on the 5^+ state at 328.92 keV is reminiscent of the decoupled band built on the $h_{11/2}$ orbital in the neighboring nucleus ^{105}Pd. The two other bands, based on the second 7^+ state (625.80 keV) and the 6^+ isomer (89.63 keV) exhibit a $\Delta I=1$ level sequence. (Since the strongest transition from the 625.8-keV 7^+ state goes to the yrast 7^+ state, the 6^+ isomer should not be considered as the bandhead for the 353-keV, 593-keV, etc., cascade.) An interesting feature of the 7^+ band is the energy staggering, i.e., the even-spin states are lower and the odd-spin states higher than they would be in a typical $\Delta I=1$ strong-coupled band. There is less energy staggering in the band based on the 6^+ isomer and the even-spin and odd spin states shift in the opposite direction. The $\Delta I=1$ transitions above the 8^+ level are much weaker in the 6^+ band than in the 7^+ band.

In the negative-parity states, the most prominent feature is a $\Delta I=1$ band with weak $\Delta I=2$ crossovers, based on the 8^- state at 874.2 keV. A conspicuous feature of this structure is the compression of the 7^- and 6^- states below the 8^- state. There is also another band with low-energy, $\Delta I=1$ γ rays, based on the 10^- state at 2441.6 keV. It is very reminiscent of "three-quasiparticle" bands in neighboring odd-mass nuclei, both in terms of the bandhead energy and the level spacings. For example, there is a $\Delta I=1$ band in ^{105}Pd based on the $\frac{17}{2}^+$ state at 2552.2 keV with γ-ray energies of 255, 313, and 349 keV.[9]

IV. ROTATIONAL MODEL CALCULATIONS

A. Calculation of energies and wave functions

The low-lying states in an odd-odd nucleus provide the purest examples of two-quasiparticle states. Unlike the case of the "two-quasiparticle" states in even-even nuclei, there can be no mixing with zero-quasiparticle states. Therefore, odd-odd nuclei present a unique opportunity to test the two-quasiparticle calculations.

We have performed two-quasiparticle-plus-symmetric-rotor calculations to interpret the various structures observed in ^{106}Ag. The calculation of energies and wave functions is similar to that of Flaum and Cline[16] except that (i) a variable moment of inertia is used to describe the energy levels of the core, and (ii) antisymmetrization of the two-particle wave function is not needed since the two odd particles are not identical. A new feature of the calculation is the use of the wave functions to calculate detailed electromagnetic transition properties—branching ratios, multipole mixing ratios, and half-lives—including the $E1$, $M1$, $E2$, and $M2$ modes.

The nucleus is treated as two odd particles coupled to a slightly deformed even-even core which is an axially symmetric ellipsoid. The

basis consists of strong-coupled rotational states built on two-particle states in a deformed potential.

$$|IMK\rangle = \left(\frac{2I+1}{16\pi^2}\right)^{1/2} [D^I_{MK}\chi^{\Omega_p}\chi^{\Omega_n} + \pi(-)^{(I+1)}D^I_{M,-K}\chi^{-\Omega_p-\Omega_n}]. \quad (1)$$

Here, Ω_p and Ω_n are projections on the symmetry axis of single-particle angular momenta $\vec{j}_p$ and $\vec{j}_n$, respectively, and π is the parity of the state. The projection K of the total angular momentum $\vec{I}$ of the nucleus is equal to that of the total *particle* angular momentum $\vec{J}$, and we have the constraints

$$K = \Omega_p + \Omega_n \text{ and } K \geq 0. \quad (2)$$

The Ω's can have any signs as long as the sum of Ω_p and Ω_n is non-negative. The D^I_{MK} are the usual rotation matrices and the χ^Ω the single-particle states, i.e., Nilsson states[17] under quasiparticle transformation.

The Hamiltonian of the system may be described as

$$H = H_{sp}(p) + H_{sp}(n) + H_{int} + H_{rot}, \quad (3)$$

where the H_{sp} parts for the two single particles are the Nilsson Hamiltonians under quasiparticle transformation. All terms from the expansion of H_{rot} are included.

$$H_{rot} = \frac{\hbar^2}{2\vartheta}|\vec{R}|^2 = \frac{\hbar^2}{2\vartheta}|\vec{I} - \vec{j}_p - \vec{j}_n|^2. \quad (4)$$

The moment of inertia ϑ in each strong-coupled band is treated in analogy with the VMI model[18] and its one-particle extension[2] by adding an "elastic energy" term $\frac{1}{2}C(\vartheta - \vartheta_0)^2$ to the Hamiltonian and applying the variational principle to the diagonal energies E_{IK},

$$\partial E_{IK}/\partial \vartheta_{IK} = 0.$$

The residual particle-particle interaction H_{int} is treated in the simplest approximation which schematically includes the splitting of the $K = |\Omega_1| \pm |\Omega_2|$ doublets, i.e., as a diagonal interaction

$$(H_{int})_{KK'} = -4G\langle\Sigma_p\rangle\langle\Sigma_n\rangle\delta_{KK'}, \quad (5)$$

where G is a constant. The expectation values $\langle\Sigma_p\rangle$ and $\langle\Sigma_n\rangle$ of the intrinsic spin projections of the particles are calculated because the corresponding quantum numbers in the Nilsson wave functions are not reliable estimates of these quantities at small deformations. Equation (5) shows that the residual interaction lowers the energy of those basis states where the intrinsic spins of the particles are coupled parallel to each other, in accordance with the conclusion of Gallagher and Moszkowski.[19]

Band mixing through the residual interaction is ignored in this simple calculation. For the majority of high-spin states considered here, the effects of the Coriolis interaction are expected[16] to be larger than the effects of residual interactions. Moreover, the form of residual interactions is not well understood. Thus their inclusion in the calculation would introduce unphysical parameters, increase computational time, and obscure the dependence of the results on the simple rotational nature of the model. However, a note of caution is necessary. The band-mixing terms of H_{rot} conserve parity and isospin of the neutron and proton separately. This produces four independent classes of states discussed below. Appropriate residual interactions could mix states from different classes but which have the same parity. In such cases even a weak residual interaction could have significant effects on states with similar energies.

The mixing of basis states is treated by diagonalizing the Hamiltonian. The final wave functions are linear combinations of the basis states,

$$|IM\nu\rangle = \sum_K f_{IK\nu}|IMK\rangle. \quad (6)$$

The quantum number ν distinguishes between different final states with the same spin and which belong to the same class. The symbol K in Eqs. (5) and (6) denotes not just the projection quantum number but a whole set of quantum numbers characterizing a two-particle state, i.e.,

$$\{K\} = K, \Omega_p, \Omega_n, \alpha_p, \alpha_n,$$

where the parameters α distinguish between different Nilsson states with the same value of Ω.

B. Calculation of transition properties

The calculation of transition properties is similar to that of Reich *et al.*[20] Only collective- and single-particle transitions are considered, i.e., transitions in which both particles change states are ignored. This enables us to express a transition amplitude between two-particle basis states in terms of the Nilsson one-particle amplitudes.[17] The intrinsic part of the multipole operator is separated into the proton and neu-

tron parts.

$$\underline{M}(\lambda,\mu)=\underline{M}_p(\lambda,\mu)+\underline{M}_n(\lambda,\mu), \tag{7}$$

where $\underline{M}_p$ and $\underline{M}_n$ are the usual single-particle operators.[4]

The reduced matrix element of this operator between the initial and final two-particle basis states [Eq. (1)] is

$$[(2I_i+1)/(2I_f+1)]^{1/2}\sum_{1=p,n}\left\{\delta_{\Omega_{1i},\Omega_{1f}}C(I_i,\lambda,I_f;K_i,K_f-K_i)\int\chi^{\Omega_{2f}}\underline{M}_2'(\lambda)\chi^{\Omega_{2i}}d\tau_2\right.$$
$$\left.+\pi_f(-)^{(I_f+1)}\delta_{\Omega_{1i},-\Omega_{1f}}C(I_i,\lambda,I_f;K_i,-K_f-K_i)\int\chi^{-\Omega_{2f}}\underline{M}_2'(\lambda)\chi^{\Omega_{2i}}d\tau_2\right\}.$$

Indices 2 and 1 here denote the "active" particle, i.e., the one that undergoes a transition, and the "passive" particle, respectively. The prime over the operator indicates that it is a function of the intrinsic coordinates. The summation is carried out over the proton and the neutron. The integrals in the above equation, to be called $T(K_i\to K_f)$, are the same as the one-particle integrals of Nilsson. These have been expressed in Ref. 17 in terms of the G and $b\times G$ terms, which correspond to the $|\Omega|\to|\Omega'|$ and $|\Omega|\to-|\Omega'|$ types of transitions, respectively. In the present case, since the Ω's can have positive or negative signs, T can be equal to either G or $b\times G$, with an appropriate phase factor. Table II, which is a generalization of a description given by Reich *et al.*,[20] summarizes the relationship between T and the Nilsson G and $b\times G$ terms for various cases of Ω combinations. The integrals T are functions of radial wave functions, compositions of the initial and final Nilsson states in the spherical $(N1\Lambda\Sigma)$ basis, and the g factors g_l and g_s corresponding to orbital and spin angular momenta. The dependence of the transition amplitude on

TABLE II. Summary of the relations between quantities relevant to transitions between two-particle states and the Nilsson G and $b\times G$ terms. The G and $b\times G$ terms below should be read as $G(|\Omega_{2i}|\to|\Omega_{2f}|)$ and $bG(|\Omega_{2i}|\to|\Omega_{2f}|)$, respectively. π_{1f} and π_{2f} denote the parities of the two particles in the final state. π_f denotes the overall parity of the final state: $\pi_f=\pi_{1f}\pi_{2f}$.

$\Omega_{1i}=\pm\Omega_{1f}$	Signs of Ω_{2i}	Signs of Ω_{2f}	$T(K_i\to K_f)$	CG
			$E\lambda$ transitions	
$\Omega_{1i}=\Omega_{1f}$	+	+	$G_{E\lambda}$	$C(I_i,\lambda,I_f;K_i,K_f-K_i)$
	−	−	$G_{E\lambda}$	
	+	−	$(-)^{(\lvert\Omega_{2f}\rvert+1/2)}\pi_{2f}b_{E\lambda}G_{E\lambda}$	
	−	+	$(-)^{(\lvert\Omega_{2f}\rvert+1/2)}\pi_{2f}b_{E\lambda}G_{E\lambda}$	
$\Omega_{1i}=-\Omega_{1f}$	+	+	$(-)^{(\lvert\Omega_{2f}\rvert+1/2)}\pi_{2f}b_{E\lambda}G_{E\lambda}$	$(-)^{(I_f+1)}\pi_f C(I_i,\lambda,I_f;K_i,-K_f-K_i)$
	−	−	$(-)^{(\lvert\Omega_{2f}\rvert+1/2)}\pi_{2f}b_{E\lambda}G_{E\lambda}$	
	+	−	$G_{E\lambda}$	
	−	+	$G_{E\lambda}$	
			$M\lambda$ transitions	
$\Omega_{1i}=\Omega_{1f}$	+	+	$G_{M\lambda}$	$C(I_i,\lambda,I_f;K_i,K_f-K_i)$
	−	−	$-G_{M\lambda}$	
	+	−	$(-)^{(\lvert\Omega_{2f}\rvert+1/2)}\pi_{2f}b_{M\lambda}G_{M\lambda}$	
	−	+	$(-)^{(\lvert\Omega_{2f}\rvert-1/2)}\pi_{2f}b_{M\lambda}G_{M\lambda}$	
$\Omega_{1i}=-\Omega_{1f}$	+	+	$(-)^{(\lvert\Omega_{2f}\rvert+1/2)}\pi_{2f}b_{M\lambda}G_{M\lambda}$	$(-)^{(I_f+1)}\pi_f C(I_i,\lambda,I_f;K_i,-K_f-K_i)$
	−	−	$(-)^{(\lvert\Omega_{2f}\rvert-1/2)}\pi_{2f}b_{M\lambda}G_{M\lambda}$	
	+	−	$G_{M\lambda}$	
	−	+	$-G_{M\lambda}$	

spins I_i and I_f is contained in the CG terms (Table II, last column), which are just Clebsch-Gordan coefficients with appropriate phase factors.

The final results for the transition amplitude for various multipoles may now be expressed in the following convenient forms:

$$A_{\mathrm{Nil}}(M1, I_i K_i \to I_f K_f) = \sum_{p,n} 1.03\times 10^6 E_\gamma^{3/2} \times T_{M1}(K_i \to K_f)\,\mathrm{CG}\,P_{if}\,, \tag{9a}$$

$$A_{\mathrm{Nil}}(M2; I_i K_i \to I_f K_f) = \sum_{p,n} 1.18\times 10^3 A^{1/6} E_\gamma^{5/2} \times T_{M2}(K_i \to K_f)\,\mathrm{CG}\,P_{if}\,, \tag{9b}$$

$$A_{\mathrm{Nil}}(E1, I_i K_i \to I_f K_f) = \sum_{p,n} 1.96\times 10^7 (1 - Z/A) A^{1/6} E_\gamma^{3/2} \times T_{E1}(K_i \to K_f)\,\mathrm{CG}\,P_{if}\,, \tag{9c}$$

$$A_{\mathrm{Nil}}(E2, I_i K_i \to I_f K_f) = \sum_{p,n} 2.24\times 10^4 (1 + Z/A^2) A^{1/3} E_\gamma^{5/2} \times T_{E2}(K_i \to K_f)\,\mathrm{CG}\,P_{if}\,, \tag{9d}$$

where the factor P_{if} is the usual pairing correction factor obtained from quasiparticle transformation in the BCS approximation:

$$P_{if} = u(\Omega_{2i})u(\Omega_{2f}) \pm v(\Omega_{2i})v(\Omega_{2f})\,, \tag{10}$$

the + sign being used for magnetic transitions and the − sign for electric transitions. Transition energy E_γ is in MeV, and the resulting amplitude is obtained in cgs units.

Since an intraband G_{E2} is proportional to the quadrupole moment of the single particle, the collective part of $E2$ transitions is included simply by adding the effect of the quadrupole moment of the core, Q_0, to the G_{E2} for each *intraband* transition, i.e.,

$$G_{E2}(p) + G_{E2}(n) \to G_{E2}(p) + G_{E2}(n) + C_1 Q_0\,. \tag{11}$$

The constant C_1 has been calculated[4] as

$$C_1 = 4.936\times 10^{25} A^{-1/3}\,, \tag{12}$$

and the intrinsic quadrupole moment[17] depends upon the deformation parameter δ

$$Q_0 = 0.8\,ZR^2\delta(1 + 2\delta/3)\,, \tag{13}$$

R being the nuclear radius. Since the collective component of $E2$ transitions is calculated semiempirically, it need not be corrected for pairing effects. The small collective part of $M1$ is included by replacing g_l and g_s by $g_l - g_R$ and $g_s - g_R$, respectively, where g_R, the g factor associated with core rotation, is taken as Z/A. The final transition amplitude between the Coriolis-mixed two-quasiparticle states $|I_i\nu_i\rangle$ and $|I_f\nu_f\rangle$ may be calculated by summing over all initial and final basis states,

$$A(\lambda, I_i\nu_i \to I_f\nu_f) = \sum_{K_i K_f} \{f_{I_i K_i \nu_i} f_{I_f K_f \nu_f} A_{\mathrm{Nil}}(\lambda, I_i K_i \to I_f K_f)\}. \tag{14}$$

The transition probability, the mixing ratio, and the reduced transition probability can readily be calculated from this transition amplitude

$$W(\lambda, I_i\nu_i \to I_f\nu_f) = |A(\lambda, I_i\nu_i \to I_f\nu_f)|^2\,, \tag{15}$$

$$\delta = \frac{A(2, I_i\nu_i \to I_f\nu_f)}{A(1, I_i\nu_i \to I_f\nu_f)}\,, \tag{16}$$

and

$$B(\lambda, I_i\nu_i \to I_f\nu_f) = \frac{\lambda[(2\lambda+1)!!]^2\hbar}{8\pi(\lambda+1)}\left(\frac{c}{\omega}\right)^{2\lambda+1} A(\lambda, I_i\nu_i \to I_f\nu_f)^2\,. \tag{17}$$

The mixing ratio is defined in the convention of Krane and Steffen.[21] It should be emphasized that in order to calculate the transition amplitudes correctly, particularly in sign, the phases of all the Nilsson wave functions, the two-particle wave functions, the Coriolis mixing amplitudes, and the quantities $T(K_i \to K_f)$ and CG must be mutually consistent.

C. R and J projections

An understanding of the coupling of various angular momenta is facilitated by transforming the wave function $|IM\nu\rangle$ into a basis where R and J, quantum numbers corresponding to the core angular momentum and the total particle angular momentum, respectively, are good quantum numbers. A straightforward generalization of the procedure of Ref. 2 gives the relation

$$\langle IM\nu R j_p j_n J | IM\nu\rangle = \frac{1}{\sqrt{2}} \sum_K f_{IK\nu} c^{\Omega_p}_{j_p} c^{\Omega_n}_{j_n} (-)^{J-K}\, C(I, J, R; K, -K) C(j_p, j_n, J; \Omega_p, \Omega_n)\{1 + (-)^R\}\,, \tag{18}$$

where the coefficients c are the expansion coefficients of the Nilsson wave function in the spherical basis $|Nlj\Omega\rangle$. The R distributions can now be obtained by summation of the squares of the overlap [Eq. (18)] over all possible $j_p j_n J$; similarly, the J distributions can be obtained by summation over $j_p j_n R$. Note that because of the axial symmetry only even values of R are al-

lowed. However, all integral values of J from 0 to $(j_{p_{max}}+j_{n_{max}})$ are permitted.

D. Choice of basis and parameters

The calculation was divided into four cases, $A(+\ +)$, $B(-\ -)$, $C(-\ +)$, and $D(+\ -)$, where the two signs denote the parities of the odd neutron and odd proton, respectively. In principle, all the basis states used in the calculations for the neighboring odd-A nuclei (^{105,107}Ag, ^{105}Pd, and ^{107}Cd) should be included in the basis for the two-particle calculation. For example, there are seven Nilsson neutron states which contributed substantially to the positive-parity states in ^{105}Pd. Similarly, five positive-parity Nilsson proton states were used for ^{105}Ag calculations. Therefore, the basis for ^{106}Ag, case A (+ +), should consist of $7\times5\times2=70$ two-particle states, where the factor 2 arises from the two possible relative orientations of the projections Ω_p and Ω_n. This would be an inconveniently large basis. Therefore, for each of the four parity combinations, an initial calculation was performed with the full basis. Then the basis was truncated to 25 states considering magnitudes of the mixing amplitudes.

There are a large number of input parameters to the two-quasiparticle calculation. In the absence of constraints, these could be varied artificially to fit the data, but that would not be physically meaningful. Therefore, we have constrained all the parameters to the values needed to reproduce successfully the features of neighboring odd-A nuclei.

The parameters used in the present calculations are listed in Table III. Single-particle states were generated using the standard Nilsson calculation.[17] The Nilsson model parameters κ and μ, and the Fermi surfaces λ and pairing gaps Δ for the proton and neutron states were the same as in the odd-A cases. The VMI parameter ϑ_0 was set equal to zero as in all the odd-A nuclei in this region. Parameter C, which determines the scale of energies, depends upon the extent of truncation of the basis. The values of C used in this calculation were also close to those used for neighboring odd-A nuclei. No attenuation of the Coriolis or recoil terms was needed.

V. DISCUSSION AND INTERPRETATION

In spite of its simplicity, the model described in the preceding section provides a good description of the structure of ^{106}Ag. In most cases, a calculated state has been identified with an experimental state only if there is agreement of both energy and branching ratios. The configurations of the calculated states are then used to interpret the structure of the nucleus.

Table IV describes the calculated branching ratios, $B(EM\lambda)$ values, and half-lives associated with various states. Table V compares the calculated and experimental γ-ray mixing ratios.

TABLE III. Parameters used in the calculation. $\delta=0.12$.

Particle	Shell number	κ	μ	λ (MeV)	Δ (MeV)	Nilsson states (single-particle energies in MeV) 1	2	3	4	5	6
	5	0.064	0.35	46.3	1.1	$\frac{1}{2}^-[550]$	$\frac{3}{2}^-[541]$	$\frac{5}{2}^-[532]$	$\frac{7}{2}^-[523]$		
						(46.53)	(46.78)	(47.25)	(47.91)		
n	4	0.07	0.35	46.3	1.1	$\frac{1}{2}^+[420]$	$\frac{1}{2}^+[431]$	$\frac{3}{2}^+[411]$	$\frac{3}{2}^+[422]$	$\frac{5}{2}^+[402]$	$\frac{5}{2}^+[413]$
						(45.26)	(44.12)	(46.03)	(45.05)	(46.99)	(46.30)
	4	0.067	0.43	41.2	1.5	$\frac{1}{2}^+[440]$	$\frac{3}{2}^+[431]$	$\frac{5}{2}^+[422]$	$\frac{7}{2}^+[413]$	$\frac{9}{2}^+[404]$	
						(39.61)	(39.92)	(40.48)	(41.25)	(42.19)	
p	3	0.06	0.43	41.2	1.5	$\frac{1}{2}^-[301]$	$\frac{1}{2}^-[310]$	$\frac{3}{2}^-[301]$	$\frac{3}{2}^-[312]$	$\frac{5}{2}^-[303]$	
						(40.29)	(37.92)	(39.09)	(38.13)	(39.41)	

Case	Parity Neutron orbital	Proton orbital	Overall	Range of K	ϑ_0	C
A	+	+	+	0–7	0.0	0.1
B	–	–	+	0–6	0.0	0.045
C	–	+	–	0–8	0.0	0.1

TABLE IV. Branching ratios and half-lives of states in ^{106}Ag calculated using the rotational model.

Initial energy (keV)	I_i^π	I_f^π	Final energy (keV)	Calculated $B(E1)$ or $B(M1)$ (Weisskopf units)	Calculated $B(E2)$ or $B(M2)$ (Weisskopf units)	Branching ratios obs	Branching ratios calc	Calculated half-life (psec)
				Case A				
332.64	7^+_α	6^+_α	89.63	0.50	12.2	1.00	1.00	3.0
961.7	8^+_α	7^+_α	332.64	0.03	24.4	0.75	0.79	1.7
		6^+_α	89.63		3.2	0.25	0.15	
		7^+_β	625.80	0.023	4.6×10^{-3}	0.00 [a]	0.06	
		6^+_β	542.6		0.25	0.00	0.00	
1387.5	9^+_α	8^+_α	961.7	0.017	26.0	0.00	0.15	1.8
		7^+_α	332.64		6.2	1.00	0.77	
		8^+_β	979.09	0.015	4.6×10^{-4}	0.00 [a]	0.08	
		7^+_β	625.80		0.024	0.00	0.00	
		9^-	1044.0	1.2×10^{-8}	6.9×10^{-3}	0.00	0.00	
		8^-	874.0	6.4×10^{-10}	3.9×10^{-3}	0.00	0.00	
2115	10^+_α	9^+_α	1387.5	8.0×10^{-3}	23.5	0.00 [a]	0.26	0.65
		8^+_α	961.7		10.0	1.00	0.69	
		10^+_β	1902.5	0.024	0.067	0.00	0.01	
		9^+_β	1572.5	9.2×10^{-3}	0.55	0.00	0.04	
		8^+_β	979.09		7.8×10^{-3}	0.00	0.00	
		9^-	1044.0	2.4×10^{-11}	4.5×10^{-3}	0.00	0.00	
		8^-	874.0		3.5×10^{-4}	0.00	0.00	
2571.8	11^+_α	10^+_α	2115	7.5×10^{-3}	21.0	0.00	0.03	0.56
		9^+_α	1387.5		13.3	1.00	0.92	
		10^+_β	1902.5	7.0×10^{-3}	1.1×10^{-4}	0.00	0.05	
		9^+_β	1572.5		2.0×10^{-3}	0.00	0.00	
542.6	6^+_β	7^+_α	332.64	6.8×10^{-3}	0.51	0.37	0.02	5.1
		6^+_α	89.63	0.046	0.024	0.63	0.98	
625.80	7^+_β	6^+_β	542.6	8.1×10^{-3}	14.2	0.00	0.00	11.6
		7^+_α	332.64	0.044	0.029	0.65	0.58	
		6^+_α	89.63	5.0×10^{-3}	0.56	0.35	0.42	
979.09	8^+_β	7^+_β	625.80	0.098	19.5	1.00	0.93	4.6
		6^+_β	542.6		10.0	0.00	0.04	
		7^+_α	332.64	1.7×10^{-4}	0.015	0.00	0.01	
		6^+_α	89.63		0.18	0.00	0.02	
1572.5	9^+_β	8^+_β	979.09	0.058	17.9	0.53	0.60	0.96
		7^+_β	625.80		9.9	0.47	0.38	
		9^+_α	1387.5	0.037	0.048	0.00	0.01	
		8^+_α	961.7	1.2×10^{-3}	0.075	0.00	0.01	
		7^+_α	332.64		7.0×10^{-3}	0.00	0.00	

TABLE IV. (*Continued.*)

Initial energy (keV)	I_i^π	I_f^π	Final energy (keV)	Calculated $B(E1)$ or $B(M1)$ (Weisskopf units)	Calculated $B(E2)$ or $B(M2)$ (Weisskopf units)	Branching ratios obs	Branching ratios calc	Calculated half-life (psec)
1902.5	10_β^+	9_β^+	1572.5	0.18	12.6	0.35	0.35	1.2
		8_β^+	979.09		15.4	0.65	0.65	
		9_α^+	1387.5	6.6×10^{-5}	0.011	0.00	0.00	
		8_α^+	961.7		0.018	0.00	0.00	
2774.5	11_β^+	10_β^+	1902.5	0.05	10.4	1.00[a]	0.43	0.24
		9_β^+	1572.5		16.1	0.00	0.51	
		11_α^+	2571.8	0.044	0.022	0.00	0.01	
		10_α^+	2115	0.017	0.34	0.00	0.05	
		9_α^+	1387.5		0.015	0.00	0.00	
3017.6	12_β^+	11_β^+	2774.5	0.21	7.6	0.00	0.07	0.51
		10_β^+	1902.5		20.1	1.00	0.93	
				Case B				
721.5	7_α^+	5_α^+	328.92		29.0	1.00	1.00	69.0
1450.3	9_α^+	8_β^+	1175[b]	0.13	0.055	0.00	0.27	6.1
		7_α^+	721.3		31.0	1.00	0.73	
2376.0	11_α^+	10_β^+	1844[b]	0.12	0.022	0.00	0.40	0.51
		9_α^+	1450.3		32.7	1.00	0.60	
768.8	6_β^+	5_α^+	328.92	0.024	0.16	1.00	1.00	10.7
				Case C				
765.15	6^-	6_β^+	542.6	2.6×10^{-9}	8.5×10^{-3}	0.03	0.01	2.0×10^5
		7_α^+	332.64	2.8×10^{-11}	4.3×10^{-7}	0.03	0.02	
		6_α^+	89.63	2.8×10^{-9}	5.5×10^{-3}	0.92	0.91	
		5_α^+	328.92	7.4×10^{-10}	2.2×10^{-3}	0.03	0.06	
829.3	7^-	6^-	765.15	3.02	13.9	0.81	1.00	27.7
		7_α^+	332.64	4.2×10^{-9}	2.2×10^{-4}	0.14	0.00	
		6_α^+	89.63	9.6×10^{-8}	0.013	0.05	0.00	
874.2	8^-	7^-	829.3	2.1	12.0	0.83	0.99	114.7
		6^-	765.15		0.026	0.00	0.00	
		7_α^+	332.64	7.6×10^{-8}	1.8×10^{-3}	0.17	0.01	
1044.0	9^-	8^-	874.2	1.33	20.9	1.00	1.00	3.4
		7^-	829.3		2.0	0.00	0.00	
1420.8	10^-	9^-	1044.0	0.91	19.1	0.93	0.98	0.44
		8^-	874.2		14.0	0.07	0.02	
1764.2	11^-	10^-	1420.8	0.72	15.9	0.82	0.87	0.66
		9^-	1044.0		18.8	0.18	0.13	
2254.4	12^-	11^-	1764.2	0.75	13.3	0.85	0.90	0.22
		10^-	1420.8		21.6	0.15	0.10	
2745.6	13^-	12^-	2254.4	0.60	11.7	0.75	0.79	0.34
		11^-	1764.2		23.6	0.25	0.21	

TABLE IV. (*Continued.*)

[a] There is some evidence for a weak presence of this γ ray in our data, but it is not conclusive.

[b] Experimental energy is not known; calculated value has been used for E_γ.

The square of the mixing ratio gives the ratio of the $\lambda=2$ and $\lambda=1$ contributions to the transition probability. [It may be noted that the Weisskopf single particle units for the reduced transition probabilities, used in Table IV, are such that the numerical values quoted for quantities $B(M1)$ and $B(E2)$ do not provide a direct way of comparing the relative strengths of the two modes in a given mixed transition.] When available, experimental transition energies were used for E_γ in Eq. (9) to calculate the transition properties. However, where the relevant initial or final state was not observed, calculated energies were used to get an estimate of branching ratios and mixing ratios. Figure 5 presents the calculated energy levels and compares them with the observed states. States connected by strong electromagnetic transitions are grouped together in Fig. 5 and described as a "band." The zero-energy point for each calculated band has been adjusted so that the energies of states marked with asterisks match with the corresponding experimental energies. (The adjustments needed in all cases agreed within 350 keV.) There are many components contributing to any of the calculated wave functions, each component consisting of a neutron Nilsson state and a proton Nilsson state with their Ω's added parallel or antiparallel to each other. A summary of the prominent components and J projections for the calculated states is given in Table VI. The header table placed above each part of the main table gives information about the prominent basis states. A number in any column in the main table is the probability of a particular configuration in the final state.

TABLE V. γ-ray mixing ratios in ^{106}Ag calculated using the rotational model.

I_i^π	I_f^π	E_γ (keV)	Mixing ratio δ obs	calc
Case A				
7^+_α	6^+_α	243	$-0.17 \leq \delta \leq -0.12$	−0.04
8^+_α	7^+_α	629	$4 \leq \delta \leq 8$	−0.62
6^+_β	7^+_α	210	$0.0 \leq \delta \leq 0.4$	0.06
6^+_β	6^+_α	453		−0.01
7^+_β	7^+_α	293	$-0.25 \leq \delta \leq -0.08$	0.01
7^+_β	6^+_α	536	$\delta \approx 0.5$	−0.19
8^+_β	7^+_β	353	$0.03 \leq \delta \leq 0.07$	0.17
9^+_β	8^+_β	593	$0.05 \leq \delta \leq 0.25$	0.35
10^+_β	9^+_β	330		0.09
Case B				
6^+_β	5^+_α	440	$0.1 \leq \delta \leq 0.2$	−0.04
Case C				
6^-	7^+_α	223		−0.21
6^-	6^+_β	433	$-0.07 \leq \delta \leq 0.09$	−0.02
6^-	6^+_α	676	$-0.13 \leq \delta \leq 0.13$	0.45
7^-	6^-	64	$0.00 \leq \delta \leq 0.03$ [a]	0.00
7^-	7^+_α	497	$0.6 \leq \delta \leq 1.0$	0.05
7^-	6^+_α	740	$-0.2 \leq \delta \leq 0.08$	0.13
8^-	7^-	45	$-0.02 \leq \delta \leq 0.02$ [a]	0.00
8^-	7^+_α	542	$-0.02 \leq \delta \leq 0.02$	0.04
9^-	8^-	170	$0.02 \leq \delta \leq 0.06$	0.02
10^-	9^-	377	$0.02 \leq \delta \leq 0.06$	0.06
11^-	10^-	343	$-0.02 \leq \delta \leq 0.02$	0.05
12^-	11^-	490		0.07
13^-	12^-	491		0.06

[a] Deduced from data given in Ref. 7.

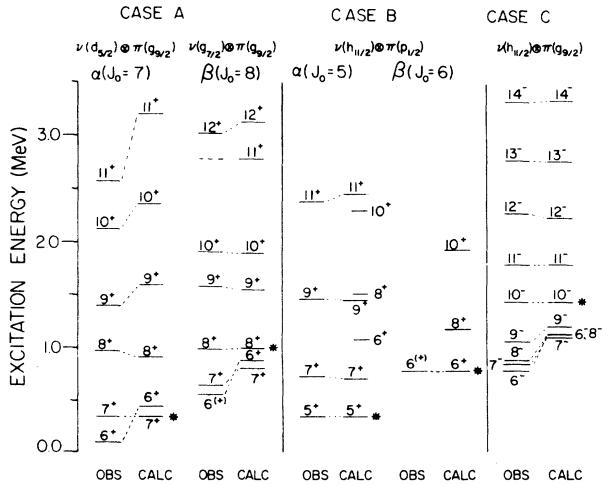

FIG. 5. Comparison of calculated and experimental energies of various states in ^{106}Ag. Calculated states are identified with observed states on the basis of their energies as well as transition properties.

TABLE VI. Summary of numerical results of the Coriolis calculation of energy levels and wave functions in ^{106}Ag. The basis states are identified by serial numbers as defined in the header table for each case. E_0 is the intrinsic energy: $E_0 = E_{sp}(n) + E_{sp}(p) + E_{int}$.

(a) Case A: $\nu(g_{7/2}, d_{5/2}) \otimes \pi(g_{9/2})$

State number	K	Nilsson states Neutron	Nilsson states Proton	Predominant spherical orbital Neutron	Predominant spherical orbital Proton	E_0 (keV)
1	7	$\frac{5}{2}^+[413]$	$\frac{9}{2}^+[404]$	$d_{5/2}$		270
2	6	$\frac{5}{2}^+[413]$	$\frac{7}{2}^+[413]$	$d_{5/2}$		−65
3	5	$\frac{5}{2}^+[413]$	$\frac{5}{2}^+[422]$	$d_{5/2}$		68
4	4	$\frac{5}{2}^+[413]$	$\frac{3}{2}^+[431]$	$d_{5/2}$		374
5	7	$\frac{5}{2}^+[402]$	$\frac{9}{2}^+[404]$	$g_{7/2}$	$g_{9/2}$	525
6	6	$\frac{5}{2}^+[402]$	$\frac{7}{2}^+[413]$	$g_{7/2}$		173
7	5	$\frac{3}{2}^+[411]$	$\frac{7}{2}^+[413]$	$g_{7/2}$		106
8	4	$\frac{3}{2}^+[411]$	$\frac{5}{2}^+[422]$	$g_{7/2}$		215
9	3	$\frac{3}{2}^+[411]$	$\frac{3}{2}^+[431]$	$g_{7/2}$		491

I^π	Energy (keV) obs	Energy (keV) calc	Amount of Coriolis mixing, $f_{IK\nu}^2$ (1)	(2)	(3)	(4)		J composition $J_0=5$	$J_0=6$	$J_0=7$	$J_0=8$
6^+_α	90	429		0.40	0.33	0.13		0.11	0.54	0.30	0.03
7^+_α	333	≡333	0.32	0.30	0.13	0.04		0.01	0.12	0.84	0.02
8^+_α	962	900	0.24	0.32	0.17	0.05		0.02	0.14	0.81	0.02
9^+_α	1388	1588	0.18	0.30	0.20	0.07		0.03	0.14	0.80	0.02
10^+_α	2115	2355	0.15	0.32	0.25	0.10		0.02	0.17	0.73	0.06
11^+_α	2572	3201	0.11	0.27	0.25	0.11		0.04	0.16	0.76	0.02
			(5)	(6)	(7)	(8)	(9)				
6^+_β	543	870		0.10	0.18	0.22	0.10	0.07	0.19	0.17	0.52
7^+_β	626	794	0.15	0.15	0.20	0.14	0.04	0.06	0.12	0.23	0.57
8^+_β	979	≡979	0.07	0.09	0.16	0.16	0.07	0.05	0.16	0.15	0.60
9^+_β	1573	1540	0.07	0.12	0.19	0.18	0.06	0.06	0.15	0.17	0.60
10^+_β	1903	1879	0.02	0.05	0.10	0.14	0.10	0.05	0.19	0.11	0.61
11^+_β	(2775)	2781	0.04	0.09	0.17	0.20	0.09	0.06	0.16	0.14	0.60
12^+_β	3018	3120	0.01	0.03	0.07	0.12	0.10	0.04	0.21	0.08	0.61

(b) Case B: $\nu(h_{11/2}) \otimes \pi(p_{1/2}, f_{5/2})$

State number	K	Nilsson states Neutron	Nilsson states Proton	Predominant spherical orbital Neutron	Predominant spherical orbital Proton	E_0 (keV)
1	2	$\frac{5}{2}^-[532]$	$\frac{1}{2}^-[301]$			491
2	2	$\frac{3}{2}^-[541]$	$\frac{1}{2}^-[301]$			517
3	1	$\frac{3}{2}^-[541]$	$\frac{1}{2}^-[301]$	$h_{11/2}$	$p_{1/2}$	299
4	1	$\frac{1}{2}^-[550]$	$\frac{1}{2}^-[301]$			371
5	0	$\frac{1}{2}^-[550]$	$\frac{1}{2}^-[301]$			293

TABLE VI. (*Continued.*)

I^π	Energy (keV) obs	calc	Amount of Coriolis mixing $f_{IK\nu}^2$ (1)	(2)	(3)	(4)	(5)	J composition $J_0=3$	$J_0=4$	$J_0=5$	$J_0=6$
5^+_α	329	≡329	0.14	0.08	0.26	0.19	0.27	0.08	0.01	0.81	0.01
7^+_α	722	702	0.14	0.09	0.25	0.19	0.27	0.07	0.01	0.81	0.01
9^+_α	1450	1444	0.13	0.09	0.24	0.19	0.27	0.07	0.01	0.79	0.01
11^+_α	2376	2456	0.13	0.10	0.23	0.19	0.26	0.06	0.01	0.74	0.02
6^+_β	(769)	≡769	0.07	0.17	0.17	0.24	0.25	0.00	0.09	0.02	0.81
8^+_β		1167	0.07	0.17	0.17	0.24	0.25	0.00	0.09	0.01	0.81
10^+_β		1918	0.07	0.16	0.17	0.24	0.25	0.00	0.09	0.01	0.81

(c) Case C: $\nu(h_{11/2})\otimes\pi(g_{9/2})$

State number	K	Nilsson states Neutron	Proton	Predominant spherical orbital Neutron	Proton	E_0 (keV)
1	7	$\frac{5}{2}^-[532]$	$\frac{9}{2}^+[404]$			470
2	6	$\frac{5}{2}^-[532]$	$\frac{7}{2}^+[413]$			527
3	6	$\frac{3}{2}^-[541]$	$\frac{9}{2}^+[404]$			279
4	5	$\frac{3}{2}^-[541]$	$\frac{7}{2}^+[413]$			336
5	5	$\frac{1}{2}^-[550]$	$\frac{9}{2}^+[404]$			195
6	4	$\frac{1}{2}^-[550]$	$\frac{9}{2}^+[404]$	$h_{11/2}$	$g_{9/2}$	195
7	4	$\frac{1}{2}^-[550]$	$\frac{7}{2}^+[413]$			252
8	3	$\frac{3}{2}^-[541]$	$\frac{9}{2}^+[404]$			279
9	3	$\frac{1}{2}^-[550]$	$\frac{7}{2}^+[413]$			252
10	3	$\frac{1}{2}^-[550]$	$\frac{5}{2}^+[422]$			460

I^π	Energy (keV) obs	calc	Amount of Coriolis mixing, $f_{IK\nu}^2$ (1)	(2)	(3)	(4)	(5)	(6)	(7)	(8)	(9)	(10)	J composition $J_0=6$	$J_0=7$	$J_0=8$	$J_0=9$	$J_0=10$
6^-	765	1111		0.05	0.07	0.10	0.22	0.27	0.05	0.16	0.00	0.01	0.37	0.34	0.10	0.00	0.00
7^-	829	1085	0.07	0.05	0.20	0.01	0.27	0.19	0.00	0.07	0.03	0.01	0.16	0.41	0.34	0.06	0.00
8^-	874	1104	0.15	0.00	0.23	0.03	0.20	0.11	0.07	0.03	0.07	0.01	0.03	0.16	0.36	0.33	0.11
9^-	1044	1184	0.13	0.04	0.16	0.09	0.12	0.05	0.11	0.01	0.06	0.04	0.01	0.04	0.24	0.46	0.24
10^-	1421	≡1421	0.11	0.06	0.12	0.12	0.08	0.04	0.11	0.01	0.06	0.06	0.01	0.02	0.18	0.46	0.33
11^-	1764	1784	0.09	0.07	0.10	0.12	0.07	0.03	0.11	0.01	0.06	0.07	0.01	0.02	0.16	0.48	0.32
12^-	2254	2241	0.07	0.07	0.08	0.12	0.06	0.02	0.11	0.01	0.06	0.09	0.01	0.02	0.12	0.45	0.39
13^-	2746	2800	0.05	0.07	0.07	0.12	0.05	0.02	0.12	0.01	0.07	0.10	0.01	0.03	0.12	0.48	0.34
14^-	3298	3370	0.03	0.05	0.05	0.11	0.04	0.02	0.11	0.00	0.06	0.11	0.01	0.02	0.11	0.43	0.42

A. Case A: Parity combination + +

These positive-parity states have neutron configurations of $g_{7/2}$ and $d_{5/2}$ parentage and proton configurations of $g_{9/2}$ parentage. On the basis of their transition properties, the calculated states are grouped into two bands arbitrarily labeled α and β. Table IV (case A) shows that the agreement between the calculated and observed branching ratios is excellent. Although states in these two bands come out of the same calculation and must have some overlap in their wave functions, no strong interband transitions are predicted above the 7^+_β state. Also, all transitions

from these states to negative-parity states are predicted to be very weak. These results are fully in agreement with the experimental decay scheme. The α and β bands show somewhat different characteristics: while the α band is dominated (above the 7^+ state) by $\Delta I=2$ transitions, the β band shows significant $\Delta I=1/\Delta I=2$ branchings at the 9^+ and 10^+ states. The calculation reproduces this trend.

The calculated energy levels (Fig. 5) are also in good agreement with the experimental results. The calculated levels in the α band could have been closer to the observed ones if different moment of inertia parameters were used for each band. The observed energy staggering between even- and odd-spin states in the β band is reproduced. The 9^+ and 11^+ states of the α band may have been affected by mixing with the corresponding states of case B which have nearly the same energies as the former. Such mixing cannot be taken into account in our calculations, as already explained.

In general, the agreement in energies is very good for the higher members of the two bands. The lower members, e.g., the 6^+ states, are placed by the calculation at higher energies than the corresponding observed levels. The same trend will be seen in the negative-parity band too. While part of the discrepancy may be attributed to the residual interaction, such a trend also has been observed in odd-A nuclei. For instance, in ^{105,107}Ag the $7/2^+$ state, observed slightly below the $9/2^+$ bandhead, is placed slightly *above* the latter by the rotational calculation.

There were several candidates among the observed states to match the calculated state 6^+_β, all of them reasonably close in energy. However, the calculation showed that this state would decay primarily to the 6^+_α isomeric state; hence the experimental $6^{(+)}$ state at 542.6 keV was identified with the 6^+_β state.

Table VI (case A) shows that the dominant value of J_0 in all states of the α band is $J_0=7$, and in the β band is $J_0=8$. The predominant neutron configuration in the α band is $\frac{5}{2}^+$ [413] of $d_{5/2}$ parentage, and in the β band, $\frac{5}{2}^+$[402] and $\frac{3}{2}^+$ [411]—both of $g_{7/2}$ parentage. Hence, these two bands may be considered as having primarily $\nu(d_{5/2})\otimes\pi(g_{9/2})$ and $\nu(g_{7/2})\otimes\pi(g_{9/2})$ configurations, respectively, although there is a considerable mixing. The dominant J_0 values for the α and β bands from the detailed calculation correspond to aligned coupling of $d_{5/2}-g_{9/2}$ and $g_{7/2}-g_{9/2}$ particles, respectively. Thus the main feature of the calculation, i.e., bands built on 7^+ and 8^+ bandheads, can be predicted qualitatively by simply considering the available quasiparticle configurations. A direct confirmation of the $d_{5/2}-g_{9/2}$ nature of the α band is the fact that the 6^+ (89.63 keV) and 7^+ (332.64 keV) states are populated[15,7] in the ^{105}Pd(^{3}He, d)^{106}Ag reaction with an angular momentum transfer of $L=4$.

The branching ratio of the 7^+_β state was the only observable sensitive to the diagonal residual interaction. Its inclusion changed the $\Delta I=0:\Delta I=I$ branching ratio from 2:98 to 58:42, which is in good agreement with the experimental value.

B. Case B: Parity combination - -

This case includes positive-parity states constructed from basis states of the type $\nu(h_{11/2})\otimes\pi(p_{1/2})$. As in case A, two bands are predicted which again are arbitrarily labeled α and β. The $\Delta I=2$ band observed in the experiment is reproduced by the calculations as the α band seen in Fig. 5. Table IV (case B) shows that the predominant decay path of these states is expected to be $11^+\to 9^+\to 7^+\to 5^+$, as observed. $\Delta I=1$ transitions to members of the β band are not favored primarily because their transition energies would be rather small. The 6^+_α, 8^+_α, and 10^+_α states are the nonaligned members of the α band, one step away from rotation alignment. They are predicted to be significantly above the yrast line, which explains why they are not populated in heavy-ion reactions.

The $\Delta I=2$ band observed in this case is seen to be similar to the $\Delta I=2$ band in ^{105}Pd which has the same neutron configuration ($h_{11/2}$). The low-spin $p_{1/2}$ proton simply acts as a spectator. The J projections show that the α and β bands indeed have different intrinsic configurations, i.e., they are dominated by $J_0=5$ and $J_0=6$, respectively, corresponding to antiparallel and parallel coupling of the particle spins 11/2 and 1/2.

C. Case C: Parity combination - +

The basis for these negative-parity states is the product of the neutron and proton states arising from the unique parity orbitals, $\nu(h_{11/2})$ and $\pi(g_{9/2})$. Table IV (case C) shows that the strong $\Delta I=1$ transitions observed in the whole band and the weak $\Delta I=2$ branches observed at and above the 10^- state are in excellent agreement with the calculated results. All the $\Delta I=1$ transitions are observed to have small positive mixing ratios. Table V (case C) shows that these are correctly reproduced by the calculation. Finally, the calculated energy levels (Fig. 5) also agree with the experimental levels. The compression of the energy levels at lower spins is reproduced, although in an exaggerated manner, as in case A.

All the parity-changing ($E1$-$M2$) transitions

observed experimentally were much weaker than any possible $M1-E2$ transitions depopulating the same state, even if the energy factor favored the former. This severe retardation of $E1-M2$ transitions agrees with the calculated results, and the calculated branching ratios are in the correct direction. The 6^- state, for which there are no possible $M1-E2$ decay paths, is predicted to be relatively long lived. It would be interesting to measure its half-life experimentally.

Table (VI) (case C) shows that the composition of these states in terms of basis states is not sharply focussed. However, intermediate values of K predominate, with an increasing emphasis on lower K values with increasing spin. This is because the neutron Fermi surface is near low-Ω orbitals, whereas the proton Fermi surface is near high-Ω orbitals. As the spin increases, the proton wave function becomes weighted towards orbitals of lower Ω because Coriolis interaction becomes stronger. The J composition also shows a corresponding shift toward $J_0 = 10$ with increasing spin.

D. Case D: Parity combination + -

Case D would include basis states corresponding to the product $\nu(d_{5/2}, g_{7/2}) \otimes \pi(p_{1/2}, f_{5/2})$. The calculation (not shown in the tables and Fig. 5) shows that the negative-parity states constructed from this basis would be considerably above the yrast line. This explains why they are not observed in our experiment. Two of the calculated bandheads, 3^- and 4^-, are predicted to lie in the same energy range as the lowest 3^- and 4^- states reported by Samuelson *et al.*[7]

E. Four-quasiparticle states

The experimental decay scheme (Fig. 3) includes a $\Delta I = 1$ band based on the 10^- state at 2441.6 keV. The energies of these states are not consistent with any of the calculated two-quasiparticle states. The decay of the 10^- bandhead to many different states also shows that its structure is not closely related to the observed two-quasiparticle states. The energy and spin of the bandhead suggest that this band may have a four-quasiparticle structure. $\Delta I = 1$ bands with bandhead energies, energy spacings, and transition properties similar to this band have also been observed in the neighboring odd-A nuclei ^{105}Pd (Ref. 9) and ^{105,107}Ag (Ref. 4) and interpreted as three-quasiparticle bands. However, a detailed description is not possible without a four-quasiparticle calculation.

VI. CONCLUSIONS

We have shown above that the structure of the odd-odd nucleus ^{106}Ag, although apparently very complicated, can be described in terms of the particle-plus-rotor model. Collective bands have been observed experimentally, and these have been classified by their two-particle configurations. It is expected, of course, that residual particle-particle interaction would mix states having the same parity but arising out of different neutron-proton parity combinations. However, this effect is seen to be overshadowed by the strong Coriolis interaction for high-angular-momentum states, making the model a good approximation.

This is but the latest step in a consistent pattern. Properties of states near the yrast line of odd-A transitional nuclei in the mass-100 and mass-130 regions have been shown to be in good agreement with the same simple model.[22] The most attractive feature of the model for these odd-A nuclei is that the dominant nature of collective bands observed can be predicted simply from the position of the Fermi surface in the Nilsson basis. When the Fermi surface is near low Ω values, decoupled $\Delta I = 2$ bands are likely to be seen. As particles are added the Fermi surface must move toward higher values of Ω. Observed bands then lose their $\Delta I = 2$ character and exhibit a $\Delta I = 1$ sequence which is still strongly influenced by Coriolis mixing. In the limit of the highest possible Ω values the bands, in fact, resemble strong-coupled rotational bands, since Coriolis forces are minimal. The same simple behavior has also been shown to characterize bands built on two-quasiparticle states in even-even nuclei, although predictions are complicated somewhat by the fact that Ω values for each quasiparticle must be considered separately. The limiting cases are still clear: if low-Ω orbitals are available near the Fermi surface for both quasiparticles, decoupled bands are to be expected; while if only high-Ω orbits are available, $\Delta I = 1$ bands will be seen. The intermediate case, where one quasiparticle occupies a low-Ω orbit and the other a high-Ω orbit, leads to a compromise situation where details such as dominant j values for the individual quasiparticles become important.

In the present work it has been seen that these simple arguments are applicable to the odd-odd nucleus ^{106}Ag. The observed positive-parity states fall very nearly into one of the limiting cases. One group (case A) represents the proton in high-Ω orbitals of $g_{9/2}$ parentage, and the neutron in intermediate-Ω orbitals of $d_{5/2}$ or $g_{7/2}$ paren-

tage. The expected $\Delta I=1$ bands were observed. The second group (case B) involves the neutron in low-Ω orbits of $h_{11/2}$ parentage, and the proton in the $p_{1/2}$ orbital, resulting in a decoupled band. The negative parity states (case C) correspond to an intermediate case with the proton in high-Ω orbitals and the neutron in low-Ω orbitals. This happens, in the present case, to result in a $\Delta I=1$ band. Systematics implies, however, that if the proton occupied low-Ω orbits of $g_{9/2}$ parentage, the corresponding negative parity band should become decoupled. This is not possible in Ag nuclei, but a trend towards decoupling is to be expected in lower-Z nuclei such as odd-odd Rh and Tc nuclei. The study of these elements would make an interesting test of the systematics discussed here.

The success of the model in interpreting systematic trends in a wide varity of nuclei and in predicting many details of their structure argues forcefully that rotational phenomena play a significant role in many transitional nuclei.

This work was supported by the National Science Foundation.

---

*Present address: Fusion Laboratory, Princeton University, Princeton, New Jersey 08540.

[1]Rakesh Popli, F. A. Rickey, and P. C. Simms, Phys. Rev. C 22, 1121 (1980).
[2]Hastings A. Smith, Jr., and F. A. Rickey, Phys. Rev. C 14, 1946 (1976).
[3]P. C. Simms, J. A. Grau, L. E. Samuelson, and F. A. Rickey (unpublished).
[4]Rakesh Popli, J. A. Grau, S. I. Popik, L. E. Samuelson, F. A. Rickey, and P. C. Simms, Phys. Rev. C 20, 1350 (1979).
[5]L. E. Samuelson, J. A. Grau, S. I. Popik, F. A. Rickey, and P. C. Simms, Phys. Rev. C 19, 73 (1979).
[6]M. W. Guidry, I. Y. Lee, N. R. Johnson, P. A. Butler, D. Cline, P. Colombani, R. M. Diamond, and F. S. Stephens, Phys. Rev. C 20, 1814 (1979).
[7]L. E. Samuelson, R. A. Emigh, D. E. Prull, R. E. Anderson, J. J. Kraushaar, and R. A. Ristinen, Z. Phys. A 294, 353 (1980).
[8]J. A. Grau, F. A. Rickey, G. J. Smith, P. C. Simms, and J. R. Tesmer, Nucl. Phys. A229, 346 (1976).
[9]F. A. Rickey, J. A. Grau, L. E. Samuelson, and P. C. Simms, Phys. Rev. C 15, 1530 (1977).
[10]J. A. Grau, L. E. Samuelson, F. A. Rickey, P. C. Simms, and G. J. Smith, Phys. Rev. C 14, 2297 (1976).
[11]Jin Soon Kim, Y. K. Lee, K. A. Hardy, P. C. Simms, J. A. Grau, G. J. Smith, and F. A. Rickey, Phys. Rev. C 12, 499 (1975).
[12]T. Yamazaki, Nucl. Data Sect. A 3, 1 (1967).
[13]F. E. Bertrand, Nucl. Data Sheets 13, 397 (1974).
[14]L. E. Samuelson (unpublished).
[15]R. E. Anderson, R. L. Bunting, J. D. Burch, S. R. Chinn, J. J. Kraushaar, R. J. Peterson, D. E. Prull, B. W. Ridley, and R. A. Ristinen, Nucl. Phys. A242, 93 (1975).
[16]C. Flaum and D. Cline, Phys. Rev. C 14, 1224 (1976).
[17]S. G. Nilsson, K. Dan. Vidensk. Selsk. Mat. Fys. Medd. 29, No. 16 (1955).
[18]M. A. J. Mariscotti, G. Scharff-Goldhaber, and B. Buck, Phys. Rev. 178, 1864 (1969).
[19]C. J. Gallagher and S. A. Moszkowski, Phys. Rev. 111, 1282 (1958).
[20]C. W. Reich, R. G. Helmer, and R. C. Greenwood, Nucl. Phys. A168, 487 (1971).
[21]K. S. Krane and R. M. Steffen, Phys. Rev. C 2, 724 (1970).
[22]P. C. Simms, F. A. Rickey, and R. K. Popli, Nucl. Phys. A347, 205 (1980).